

Simulating W/Z +jets production at the CERN LHC*

Frank Krauss,[†] Andreas Schälicke,[‡] Steffen Schumann,[§] and Gerhard Soff[¶]
Institute for Theoretical Physics, D-01062 Dresden, Germany

The merging procedure of tree-level matrix elements and the subsequent parton shower as implemented in the new event generator SHERPA will be validated for the example of single gauge boson production at the LHC. The validation includes consistency checks and comparisons to results obtained from other event generators. In particular, comparisons with full next-to-leading order QCD calculations prove SHERPA's ability to correctly account for additional hard QCD radiation present in these processes.

PACS numbers: 13.85.-t, 13.85.Qk, 13.87.-a

I. INTRODUCTION

The production of electroweak gauge bosons, which decay leptonically, is one of the most prominent examples for hard processes at hadron colliders and one of the first applications of perturbative QCD in such reactions. In fact, the next-to-leading order (NLO) corrections to this process in QCD, calculated by [1, 2, 3, 4, 5] provided the first calculation of such corrections for hadron collisions. Later, their production cross section has been calculated at NNLO by [6, 7]. Recently, the first distribution determined at NNLO related to these processes, namely the boson rapidity, has been calculated by [8]. In addition, there is a large number of computer programs dealing with single gauge boson production. They range from RESBOS [9], which resums soft gluon effects in these processes, to codes, that evaluate cross sections at the LO level for the production of gauge bosons accompanied by jets. Examples for the latter include specialised ones, such as VECBOS [10], and general ones, usually called parton level generators, such as COMPHEP [11], GRACE/GR@PPA [12, 13], MADGRAPH/MADEVENT [14, 15], ALPGEN [16], and AMEGIC++ [17]. Furthermore, the first package called MCFM has been made available that calculates total and differential cross sections at NLO precision for the production of gauge bosons with up to two jets [18, 19]. This reflects the importance of this particular process. At the LHC becoming operational in the near future, the gauge bosons will be produced with unprecedented rates. For instance, at luminosities of $\mathcal{L} \approx 10^{33} \text{cm}^2/\text{s}$ the production and leptonic decay of a single W boson will occur with a frequency of around 20 Hz, rendering this process a prime candidate for luminosity monitoring [21, 22, 23, 24]. Of course, these large rates will allow to measure the gauge bosons parameters, such as their masses and widths, with a precision [25, 26] beyond what could be reached at previous collider experiments [27, 28, 29, 30, 31, 32, 33, 34, 35, 36]. At the CERN LHC, the production of W and Z bosons together with jets also constitute an important background to all kinds of searches for new physics, such as supersymmetry. An example for this is the production and decay of gluinos, where the production of jets plus a Z boson decaying into neutrinos forms a major background. In a previous analysis [37] it has been shown that some results for this type of process, i.e. the production of single gauge bosons plus extra jets, as obtained by other multi-purpose event generators such as PYTHIA [38, 39], HERWIG [40, 41] or even MC@NLO [42, 43, 44] differ significantly from the results obtained by SHERPA [45]. In particular, it has been shown that already at the Fermilab Tevatron, operating at roughly 2 TeV centre-of-mass energy, the additional jets are produced at significantly larger transverse momenta. The reason for this difference is the way the different codes implement the knowledge of exact matrix elements for the production of multi-particle final states. In both, PYTHIA and HERWIG, they are included at first order in α_S through a correction of the first hard emission on the corresponding $q\bar{q} \rightarrow Vg$ or $qg \rightarrow Vq$ matrix element, where V stands for the vector boson [46, 47, 48]. In MC@NLO the full first order correction, including both, the virtual and the real parts, are matched with the parton shower. This has the additional benefit that MC@NLO reproduces correctly the total production rate of single gauge bosons and the spectrum of the first additional jet at first order in α_S . In contrast, in SHERPA a method has been implemented that consistently adds different matrix elements at the tree level for different jet multiplicities and merges them with the parton shower. The basic idea in this approach is to internally define a region of jet production (hard

[¶] deceased

*URL: <http://www.physik.tu-dresden.de/~krauss/hep/>

[†]Electronic address: krauss@theory.phy.tu-dresden.de

[‡]Electronic address: dreas@theory.phy.tu-dresden.de

[§]Electronic address: steffen@theory.phy.tu-dresden.de

parton emissions) and a region of jet evolution (soft parton emissions). The two regimes are divided by a k_{\perp} -type of jet measure [49, 50, 51]. Leading higher order effects are incorporated by reweighting the matrix elements with appropriate Sudakov form factors. Formal independence at leading logarithmic order of the overall result on the jet measure is achieved by suitable starting conditions and vetoing hard emissions inside the parton shower. This approach was presented for the first time [52] for e^+e^- collisions; it has been extended to hadronic collisions in [53]. A reformulation for dipole cascades has been presented in [54]. The algorithm is implemented in a fully automated way and in full generality in **SHERPA**, some other realisations [55, 56] proved the flexibility and the validity of the approach.

In this publication, the previous analysis [37] will be extended to the case of the CERN LHC, operating in the pp mode at 14 TeV centre-of-mass energy. In Sec. II, a number of consistency checks will focus on the independence of the results on variations of the internal jet definition and of the number of matrix elements involved. Also, the effect of scale variations in both the matrix elements and the parton shower is investigated there. Then, in Sec. III, results obtained with **SHERPA** will be contrasted to those obtained from fixed order (LO and NLO) calculations provided by **MC²FM**. Following this, different multi-purpose event generators, namely **PYTHIA**, **MC@NLO** and **SHERPA**, will be compared in Sec. IV, before the conclusions will summarise the findings.

II. CONSISTENCY CHECKS

Before comparing the results of **SHERPA** with those of other programs, some consistency checks will be performed. To do so, the dependence of some observables in reactions of the type $pp \rightarrow e^+e^- + X$ on internal parameters intrinsic for the merging procedure will be investigated. In particular, these parameters are the internal jet resolution cut Q_{cut} and the maximal number n_{max} of final state partons (giving rise to jets) described through matrix elements. The former parameter defines the transition of the matrix element domain to the phase space region covered by the parton shower during event generation. In principle, the actual value of this parameter can be chosen freely, nevertheless there exist criteria that guide such a choice. For very low values of Q_{cut} the evaluation of the matrix elements becomes very challenging and potentially inefficient once jet cuts are performed on the analysis level harder than the generation cut Q_{cut} . The upper limit is defined by the scale where jets produced by the parton shower start to disagree significantly from such produced by equivalent matrix elements. To study especially the effect of the upper limit, the values used in this analysis will range over nearly one order of magnitude, from 15 to 100 GeV. The choice of the number of matrix element partons taken into account may be steered by two aspects. First of all, n_{max} has to be sufficiently large to properly account for the phase space region the observable under consideration is sensitive to. As an example, consider the transverse momentum of the boson compared to that of the, say, third jet. It is obvious that a rather inclusive quantity such as the former may be appropriately described with lower values of n_{max} than the latter observable. On the other hand, the upper limit on n_{max} is given by the availability of the matrix elements at all and by the potentially large amount of CPU time the evaluation of multi-leg matrix elements requires. Within **SHERPA** matrix elements with up to four extra partons can be delivered for the processes under consideration in this publication. After evaluating the sensitivity of the results on the principal parameters defining the merging procedure, Q_{cut} and n_{max} , the effect of scale variations will be investigated. This, together with the dependence on Q_{cut} and n_{max} yields an estimate for the uncertainty related to predictions of **SHERPA**.

The results presented in this section were generated with the following setups: when varying the jet resolution parameter Q_{cut} , the maximal number of final state partons n_{max} has been set to $n_{\text{max}} = 3$. When studying the impact of different matrix element multiplicities, the scale Q_{cut} has been fixed to $Q_{\text{cut}} = 15$ GeV; this clearly maximises the impact of the higher order matrix elements. When scale variations are under consideration, the choice $Q_{\text{cut}} = 20$ GeV and $n_{\text{max}} = 2$ has been made.

In the following, Z -boson production will be investigated in more detail. Nevertheless, the process under consideration is $pp \rightarrow Z/\gamma^* \rightarrow e^+e^- + X$, where the full γ - Z interference is taken into account and spin correlations are fully respected. Further input parameters used and the phase space cuts applied are summarised in the appendix A. Note that the cut on the invariant mass of the lepton pair is just $m_{ee} > 15$ GeV which is rather small. The description of such low mass lepton pairs constitutes a real challenge for the description through the merging prescription. The reason is that at large $Q_{\text{cut}} = \mathcal{O}(100 \text{ GeV})$, lepton pairs with such low invariant mass clearly are softer than any jet produced through the matrix element, rendering a consistent merging a complicated task.

A. Observables related to the leptons

Starting from more inclusive observables, first of all the effect of parameter variation on lepton observables will be considered. In Fig. 1, the p_{\perp} spectra of both the lepton pair (upper row) and of the electron alone (lower row) are

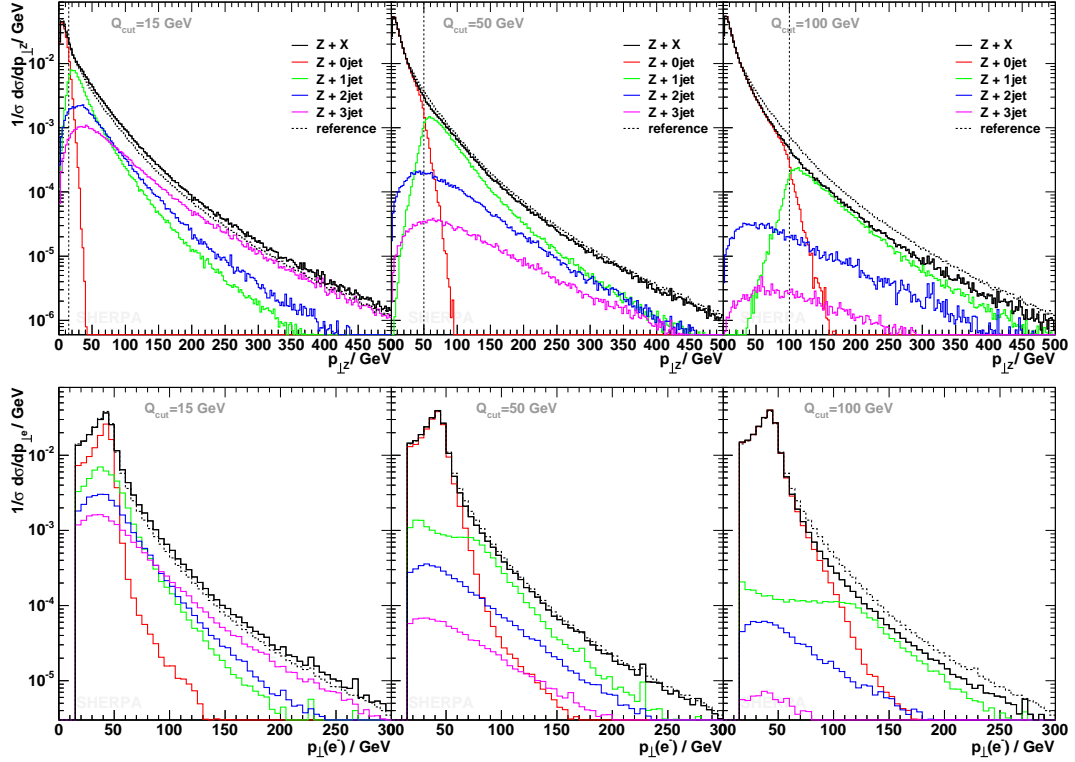


FIG. 1: $p_{\perp}(Z)$ (upper row) and $p_{\perp}(e^{-})$ (lower row) for $Q_{\text{cut}} = 15$ GeV, 50 GeV and 100 GeV (from left to right). The dashed reference spectrum has been obtained after averaging the results for $Q_{\text{cut}} = 15, 20, 30, 50, 100$ GeV.

shown for three different values of Q_{cut} : from left to right, in the columns $Q_{\text{cut}} = 15, 50, 100$ GeV, as indicated by the thin vertical lines. In each plot, the resulting spectrum is compared to a reference obtained from averaging the results for $Q_{\text{cut}} = 15, 20, 30, 50, 100$ GeV. In this and all other plots, contributions stemming from the different matrix element multiplicities are indicated through coloured lines.

Using $Q_{\text{cut}} = 15$ GeV obviously produces the hardest boson/lepton spectrum. It is the smallest cut considered here and therefore the distributions are dominated by matrix elements that in contrast to the parton shower favour rather hard parton kinematics. For very high p_{\perp} the distributions are almost completely covered by the matrix element with the highest multiplicity ($n_{\text{max}} = 3$). This shows that the LHC provides enough phase space to produce a sufficient amount of events with three and more jets of $p_{\perp} > Q_{\text{cut}}$. For the case of $Q_{\text{cut}} = 50$ GeV the situation is slightly different. The high- p_{\perp} tail is filled to an equal amount by the different multiplicities, the total sum being slightly below the reference curve. This reference curve contains three results with jet resolutions smaller than 50 GeV that somehow dominate the averaged result. The spectrum for $Q_{\text{cut}} = 100$ GeV starts to underestimate w.r.t. the reference the boson transverse momentum at $p_{\perp} \approx 35$ GeV and the lepton p_{\perp} for values larger than 60 GeV. To understand this, one has to remember that the boson transverse momentum for values below the resolution cut is almost completely covered by the parton shower. The shower description, however, is known to suffer from a lack of hard QCD radiation. This leaves not enough hard partons, the boson can recoil against. Beyond this influence of the Q_{cut} variation on the intermediate and high boson transverse momenta, it has to be noted that all curves are very smooth around the jet resolution cut. Although the cut defines a rather sharp transition from the parton shower to the matrix element domain no significant holes in the boson and lepton p_{\perp} spectra can be observed.

In Fig. 2 the pseudo-rapidity spectra of the lepton pair and the single electron are displayed; again for $Q_{\text{cut}} = 15, 50, 100$ GeV with the same way of generating the reference. While the electron observable is nearly unaltered, the differences in the η distribution of the lepton pair can be understood easily: the smaller the chosen cut, the larger the influence of the matrix elements with extra external legs. These matrix elements however prefer to produce the boson much more central than the parton shower does. This effect yields slightly tighter spectra with the central rapidities being pronounced for smaller resolution cuts.

The effect of varying n_{max} on the transverse momentum and pseudo-rapidity spectrum of the lepton pair is exhibited in Fig. 3. In this figure, results are compared for $n_{\text{max}} = 2, 3, 4$. In each plot, a reference result is given with the

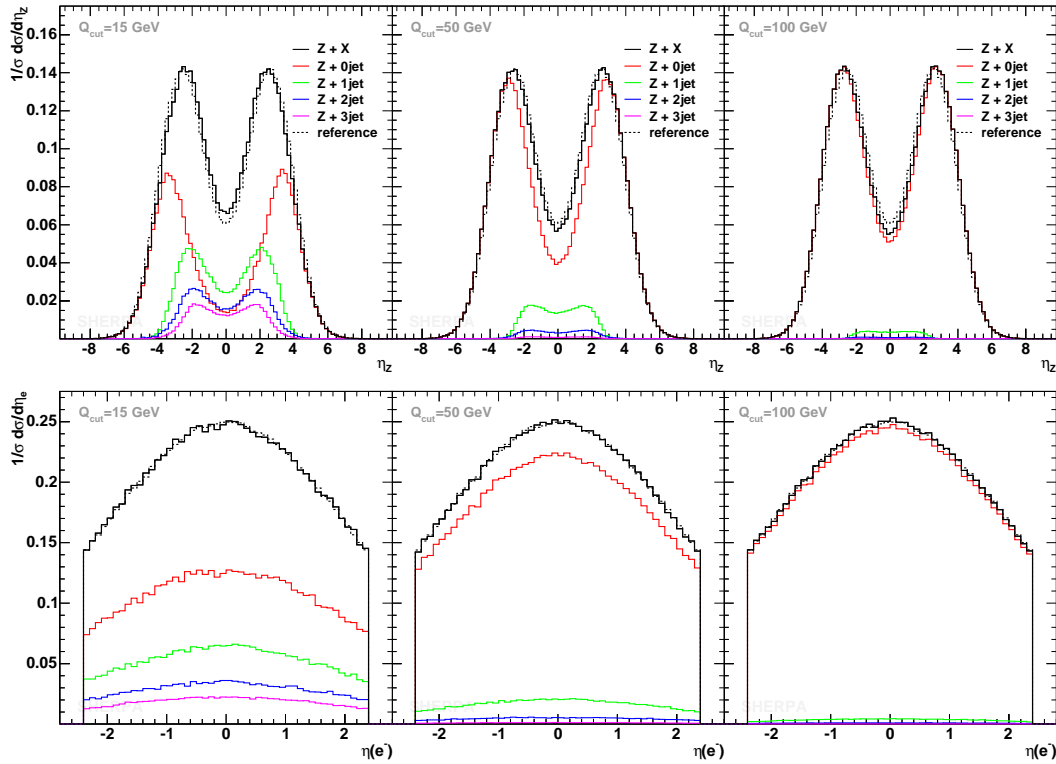


FIG. 2: $\eta(Z)$ (upper row) and $\eta(e^-)$ (lower row) for $Q_{\text{cut}} = 15$ GeV, 50 GeV and 100 GeV (from left to right). The dashed reference spectrum has been obtained after averaging the results for $Q_{\text{cut}} = 15, 20, 30, 50, 100$ GeV.

corresponding $n_{\text{max}}^{\text{ref}} = n_{\text{max}} - 1$. For the case of the p_{\perp} distribution it has already been observed that the high- p_{\perp} region is described through higher multiplicity matrix elements. As a consequence, it is the high- p_{\perp} region that is affected by the variation of n_{max} . However, while the effect is clearly noticeable when going from one to two extra partons the change becomes smaller the more matrix elements are included. From the very right plot one can conclude that considering $Z + 3$ extra parton matrix elements is a reasonable choice to simulate inclusive Z production. The change in the η distribution for different n_{max} is as expected, considering what has already been seen for varying the jet resolution. The higher multiplicity matrix elements favour the region of small $|\eta|$ yielding slightly tighter pseudo-rapidity distributions. Again, the more matrix elements have been taken into account the smaller the influence when adding an even higher multiplicity.

In comparison to what has been observed when studying gauge boson production at the Fermilab Tevatron [37], the LHC provides much more phase space for additional hard QCD radiation, enhancing the influence of higher order matrix elements. Therefore a modest value of the jet resolution parameter and the inclusion of a sufficient large number of matrix element legs is advisable for LHC analyses.

B. Jet observables

As has already been seen in the previous publication [37], a very sensitive test of the merging procedure is provided by observables based on jets. In particular, differential jet rates have turned out to be very useful, since they clearly show how the matrix elements and the parton showers interact in filling the phase space below and above the jet resolution cut. In Fig. 4, differential jet rates using the Run II k_{\perp} clustering algorithm with $R = 1$ are depicted. They signal the relevant Q value of the k_{\perp} -algorithm, where an $(n + 1)$ -jet event turns into an n -jet event. Again, the results for three different values of Q_{cut} are depicted: from left to right, in the columns $Q_{\text{cut}} = 15, 30, 100$ GeV, as indicated by the thin vertical lines. In each plot, the resulting spectrum is compared to the average of the results for $Q_{\text{cut}} = 15, 20, 30, 50, 100$ GeV. In the three rows, the differential jet rates for the $1 \rightarrow 0$, the $2 \rightarrow 1$, and for the $3 \rightarrow 2$ transition (from top to bottom) are shown. Starting the discussion with the results for $Q_{\text{cut}} = 30$ GeV, very good agreement with the reference curves can be observed. While the $3 \rightarrow 2$ transition is very smooth around the cut

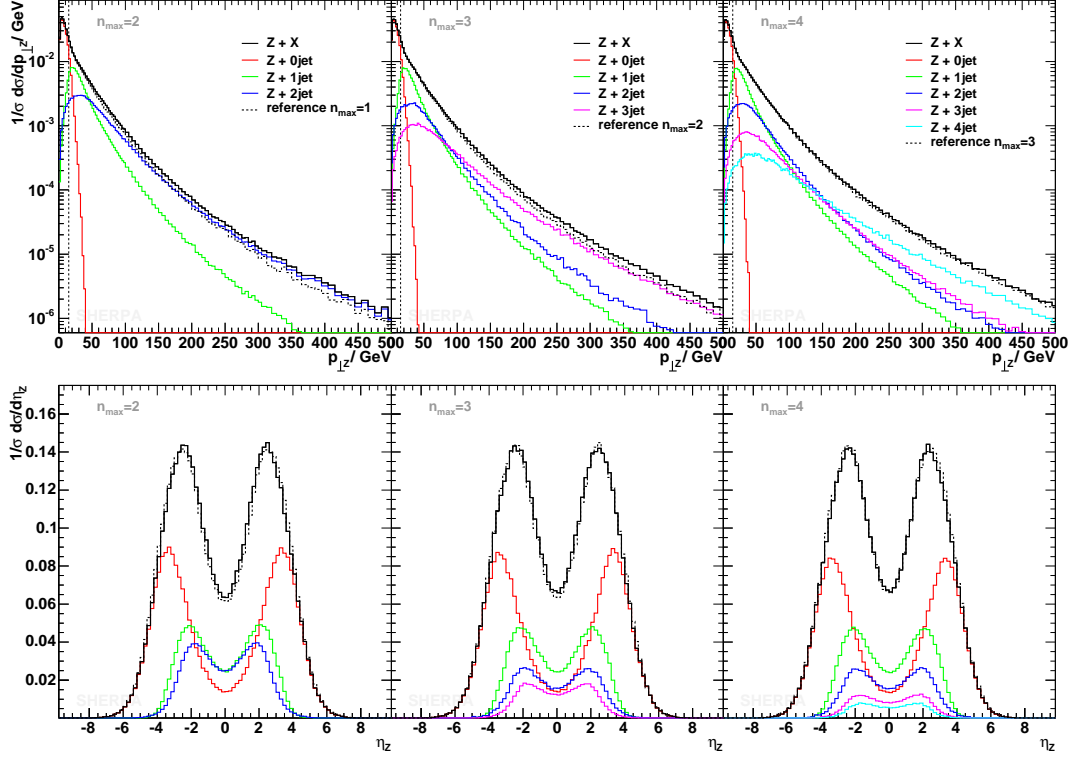


FIG. 3: $p_{\perp}(Z)$ (upper row) and $\eta(Z)$ (lower row) for $Q_{\text{cut}} = 15$ GeV and different maximal numbers (2-4, from left to right) of ME jets included. The dashed line corresponds to the maximal number of ME jets reduced by one.

the results for $1 \rightarrow 0$ and $2 \rightarrow 1$ exhibit small dips at the cut scale. Since the kinematics of the matrix elements is altered when the parton shower is attached, mismatches of the parton configurations close to the cut occur, leading to the dips. Similar structures can be observed for the case of $Q_{\text{cut}} = 100$ GeV. However, more obvious here is that the parton shower fails to fill the phase space for hard emissions up to this very large cut. For $Q_{\text{cut}} = 15$ GeV no visible dips at the cut scale are observed. Instead, this sample seems to slightly overestimate the contributions from higher order matrix elements w.r.t the reference. A small kink at Q_{cut} can be observed for the $1 \rightarrow 0$ and $2 \rightarrow 1$ transition. These residual dependences of the results on Q_{cut} may be used to tune the perturbative part of the Monte Carlo event generator.

In Fig. 5 the p_{\perp} spectrum of the jet in exclusive $Z + 1\text{jet}$ production is shown for three choices of the jet resolution scale, $Q_{\text{cut}} = 15, 50, 100$ GeV, indicated by the thin vertical line. The results are contrasted with a reference curve, again the average of results for $Q_{\text{cut}} = 15, 20, 30, 50, 100$ GeV. The jet has been defined using the Run II k_{\perp} -algorithm with a minimal jet- p_{\perp} of 20 GeV and $R = 0.4$. The smallest value of Q_{cut} presented here, namely 15 GeV, is smaller than the actual jet cut used in the analysis. Accordingly, matrix elements with more than one extra leg have a non-vanishing influence on the jet- p_{\perp} distribution. This changes as soon as Q_{cut} becomes larger than 20 GeV. For $Q_{\text{cut}} = 50$ GeV and even more for $Q_{\text{cut}} = 100$ GeV the contributions from matrix elements with $n_{\text{max}} > 1$ are almost negligible. There, only a small dip in the p_{\perp} distribution around the resolution scale can be observed. As has been seen in the transverse momentum distribution of the lepton pair, cf. Fig. 1, for $Q_{\text{cut}} = 100$ GeV, the shower is not able to fill the full phase space below the cut properly. However, the overall agreement of the three results is satisfactory, keeping in mind the large parameter range used for Q_{cut} .

To highlight the effect of taking into account different maximal numbers of final state partons through matrix elements, a two-jet correlation is exhibited in Fig. 6. There, the relative transverse angle $\Delta\phi$ between the two hardest jets in inclusive $Z + 2\text{jet}$ production is displayed; from left to right, n_{max} has set to $n_{\text{max}} = 2, 3, 4$. Each result is contrasted with a reference that has been obtained with $n_{\text{max}}^{\text{ref}} = n_{\text{max}} - 1$. From the very left plot it is clear, that the one-jet matrix element is incapable of correctly describing the $\Delta\phi$ distribution since the parton shower does not treat interferences properly. On the other hand, as soon as $n_{\text{max}} \geq 2$, the two-jet correlations are consistently described and changes due to the inclusion of higher order matrix elements are rather modest.

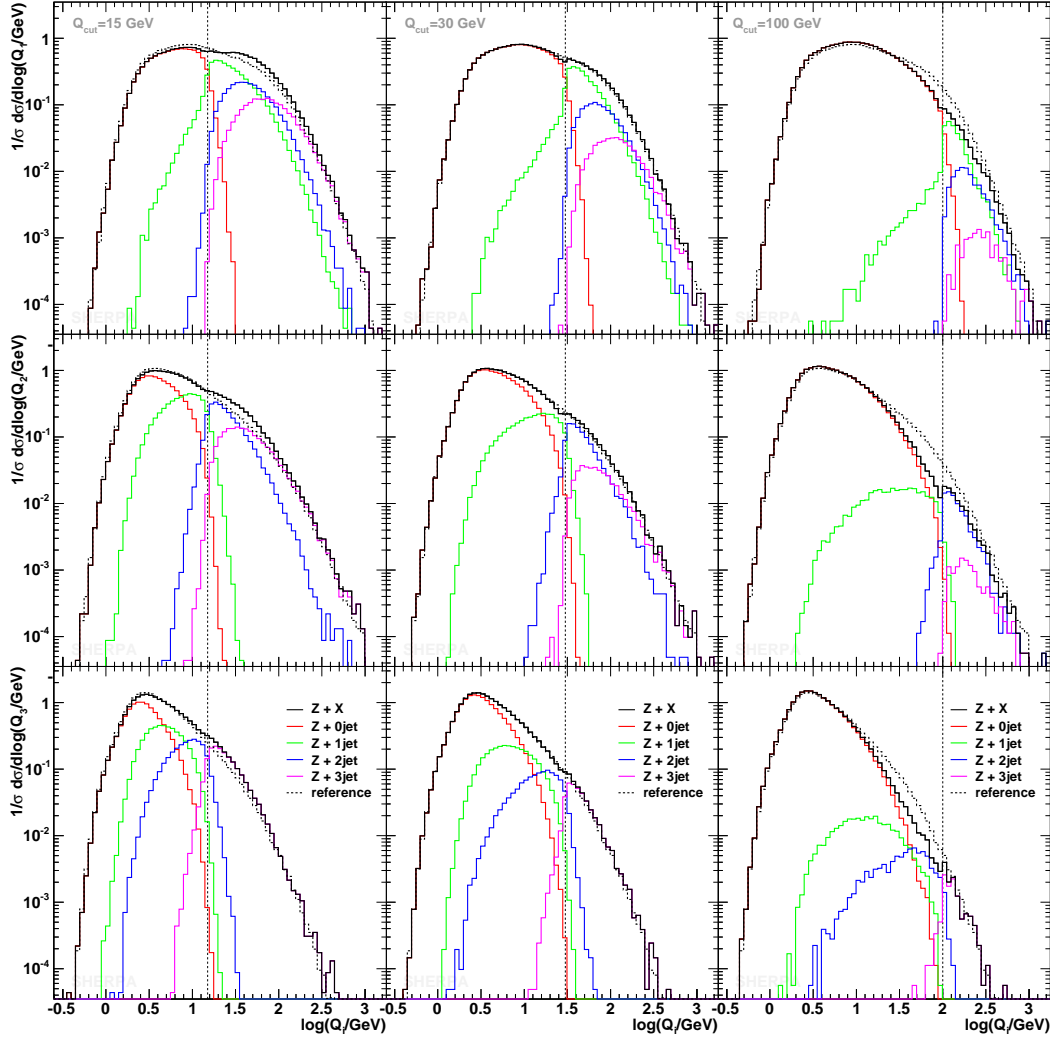


FIG. 4: Differential jet rates for the $1 \rightarrow 0$, $2 \rightarrow 1$ and $3 \rightarrow 2$ transition (top to bottom), for $Q_{\text{cut}} = 15$ GeV, 30 GeV, and 100 GeV (from left to right). The dashed reference curve in each plot is obtained after averaging the corresponding results for $Q_{\text{cut}} = 15, 20, 30, 50, 100$ GeV.

C. Variation of renormalisation and factorisation scale

The algorithm as implemented in SHERPA determines the renormalisation and factorisation scales used in a specific calculation. Of course there is some intrinsic freedom in defining the scales used for the evaluation of the PDF or the strong coupling constant. In particular, the scales used can be multiplied by constant factors, as long as this alteration is applied both in the matrix element evaluation and reweighting and in the parton shower. This restriction is due to the construction of how the leading logarithmic dependence on Q_{cut} is eliminated. The dependence of the SHERPA results with respect to such scale variations is studied in Fig. 7 and Fig. 8. Results obtained with the default scale choices are confronted with results obtained when all scales appearing in the coupling constants and PDFs are multiplied by common factors of 0.5 and 2.

In Fig. 7 the transverse momentum and pseudo-rapidity distribution of the Z/γ^* boson are depicted. For the case of the p_\perp spectrum, except for the very first bins the spectrum obtained with a factor of 0.5 (2) is always above (below) the default result. The differences are rather constant and of the order of 10–15%. As has been seen before, cf. Fig. 1 and 3, for transverse momenta above the cut scale the distribution is predominantly described by higher order matrix elements, whose scale dependence is known to be tamed with respect to the lowest order process [19]. This lowest order process, however, dominates the region of very low boson momenta. There the $2 \rightarrow 2$ cross section exhibits a strong decline when the scales become smaller. This effect potentially leads to the reversal of the discrepancies in

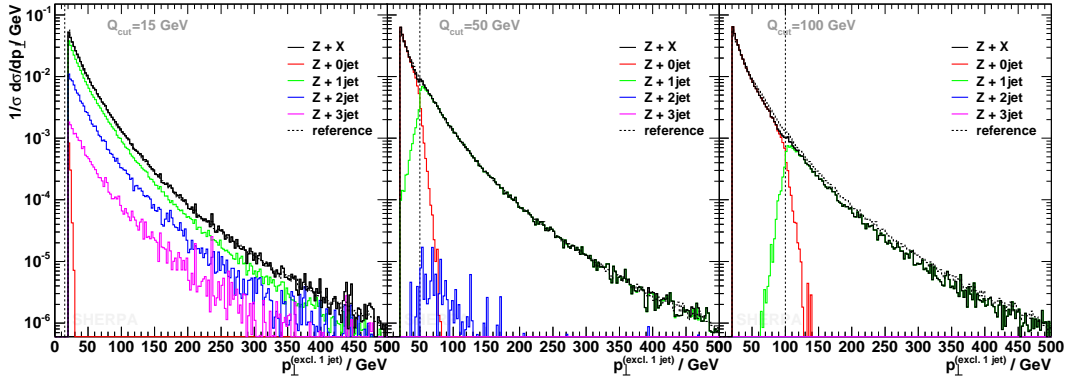


FIG. 5: p_{\perp} of the jet in exclusive $Z + 1\text{jet}$ production. For the jet definition, the Run II k_{\perp} -algorithm with $R = 0.4$ and $p_{\perp}^{\text{jet}} > 20$ GeV is used. From left to right, results for $Q_{\text{cut}} = 15, 50, 100$ GeV are contrasted with a reference: the average of the results for $Q_{\text{cut}} = 15, 20, 30, 50, 100$ GeV. The thin horizontal line indicates the jet resolution scale used.

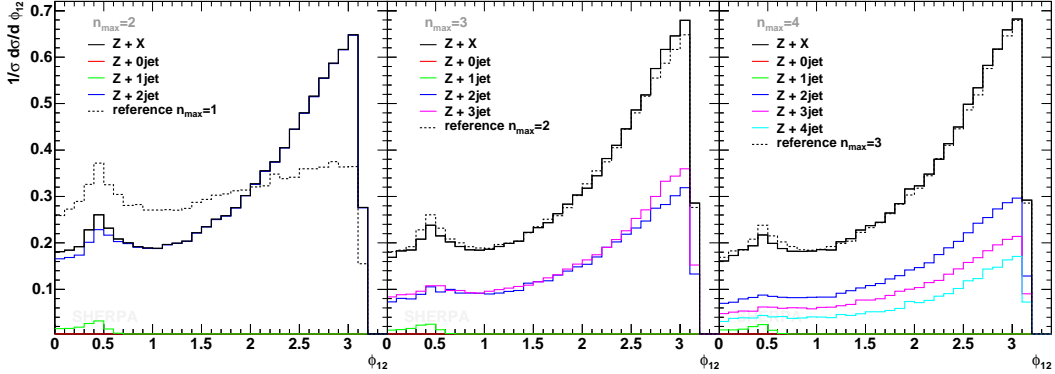


FIG. 6: $\Delta\phi_{12}$ for $Q_{\text{cut}} = 15$ GeV and different maximal numbers of ME jets included. The dashed line corresponds to the reference result obtained with $n_{\text{max}}^{\text{ref}} = n_{\text{max}} - 1$.

the soft region. The situation in the case of the pseudo-rapidity distribution is very similar. From Fig. 2 and Fig. 3 one can read off that the region of large values of $|\eta|$ is described by the parton shower attached to the $2 \rightarrow 2$ matrix element. For $|\eta| > 5$ the spectrum, where all scales have been multiplied by a factor of two, is enhanced up to 20%. A factor of 0.5 on the other hand depopulates this phase space region by up to 20%. In the intermediate range of pseudo-rapidity the deviations of the two spectra from the default scale choice are well below 10%.

In Fig. 8 the transverse momentum distribution of the hardest jet in inclusive Z/γ^* production is depicted. In contrast to the two distributions above, this result has no significant contribution from the leading order $2 \rightarrow 2$ process. Therefore, the two results obtained after scale manipulation do not cross each other. Over the whole range of jet transverse momentum the deviations of the two curves from the default result are very moderate.

It can be concluded that the predictions of SHERPA show rather mild variations over a wide range of the phase space when multiplying all scales appearing in the coupling constants and PDFs by common factors of 0.5 and 2. The largest deviations from the default choice of scales are observed in those phase space regions that are predominantly covered by the $2 \rightarrow 2$ matrix element with the parton shower attached.

III. SHERPA VS. NLO RESULTS

Having investigated the self-consistency of the merging procedure as implemented in SHERPA its parton level results are compared with those from MCFM, v. 4.0, [18, 19]. For the class of processes studied here, MCFM is capable to calculate total and fully differential cross sections at next-to-leading order in the strong coupling constant for

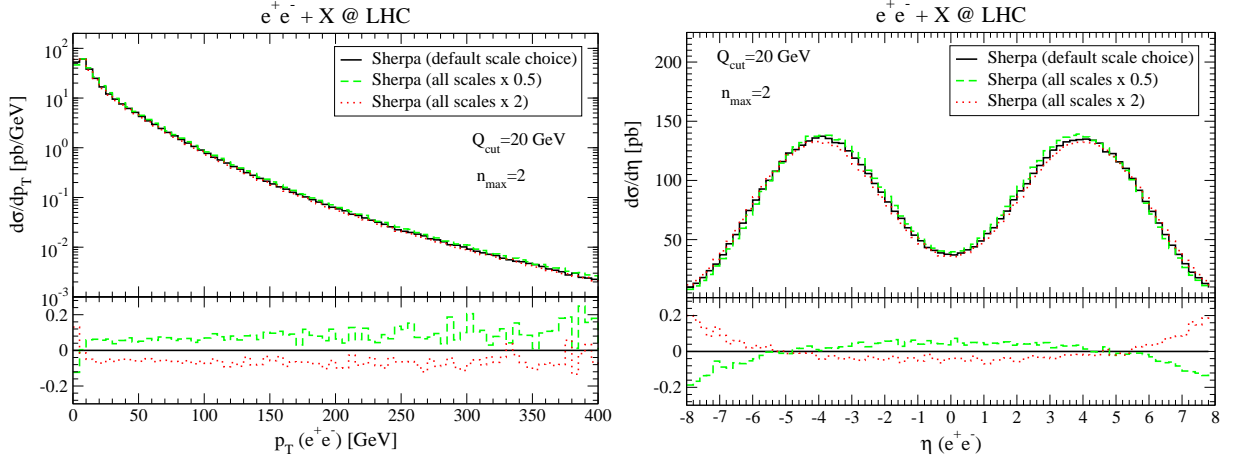


FIG. 7: The transverse momentum (left) and pseudo-rapidity (right) distribution of the boson in inclusive Z/γ^* production at the LHC and their dependence on different choices for the factorisation and renormalisation scale. Results have been obtained using $Q_{\text{cut}} = 20$ GeV and $n_{\text{max}} = 2$. The black solid lines indicate the default hadron level result of **SHERPA**. To obtain the green dashed (red dotted) line, all scales appearing in the coupling constants and the PDFs in both the matrix elements and the parton showers are multiplied by a factor of 0.5 (2). In the lower parts of the plots the variations of the results with respect to the default scale choice are presented.

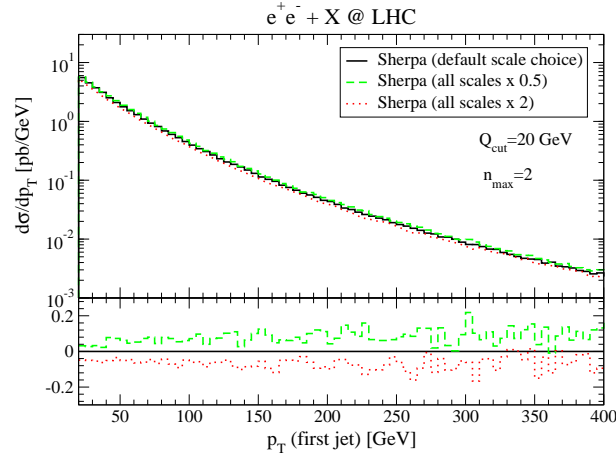


FIG. 8: The p_{\perp} spectrum of the hardest jet in inclusive Z/γ^* production at the LHC and its dependence on different choices for the factorisation and renormalisation scale. Results have been obtained using $Q_{\text{cut}} = 20$ GeV and $n_{\text{max}} = 2$. Jets are defined through the Run II k_{\perp} -algorithm with $R = 0.4$ and $p_{\perp}^{\text{jet}} > 20$ GeV. The black solid line corresponds to the default hadron level result of **SHERPA**. To obtain the green dashed (red dotted) line, all scales appearing in the coupling constants and the PDFs in both the matrix elements and the parton showers are multiplied by a factor of 0.5 (2). In the lower part of the plot the variations of the results with respect to the default scale choice are presented.

$(Z/\gamma^* \rightarrow l^+l^-) + 0, 1, 2$ and $(W^{\pm} \rightarrow l\nu_l) + 0, 1, 2$ partons. For all calculations with **MCFM** the cteq6l [20] PDF has been used, and $\alpha_S(m_Z) = 0.118$ in accordance with the value of the PDF evolution. The renormalisation and factorisation scales have been chosen to be identical with the bosons mass, i.e. $\mu_R = \mu_F = m_Z$ or $\mu_R = \mu_F = m_W$, respectively. Phase space cuts are listed in the appendix A. In contrast to a previous publication [37], this time only “inclusive” quantities are compared. For the next-to-leading order calculation this translates into an unconstrained phase space for the real higher order correction. Thus, the higher order corrections may give rise to an additional jet. The **SHERPA** results were obtained after the parton shower evolution. For the sake of a better comparison, all curves have been normalised to one, eliminating the enhancement of the cross section due to the NLO corrections.

First of all, in Figs. 9 and 10 the p_{\perp} spectra of the hardest jet in inclusive $W^+ + 1\text{jet}$, $W^- + 1\text{jet}$, and $Z/\gamma^* + 1\text{jet}$ production are exhibited. For all cases, results at leading and at next-to-leading order were contrasted with results

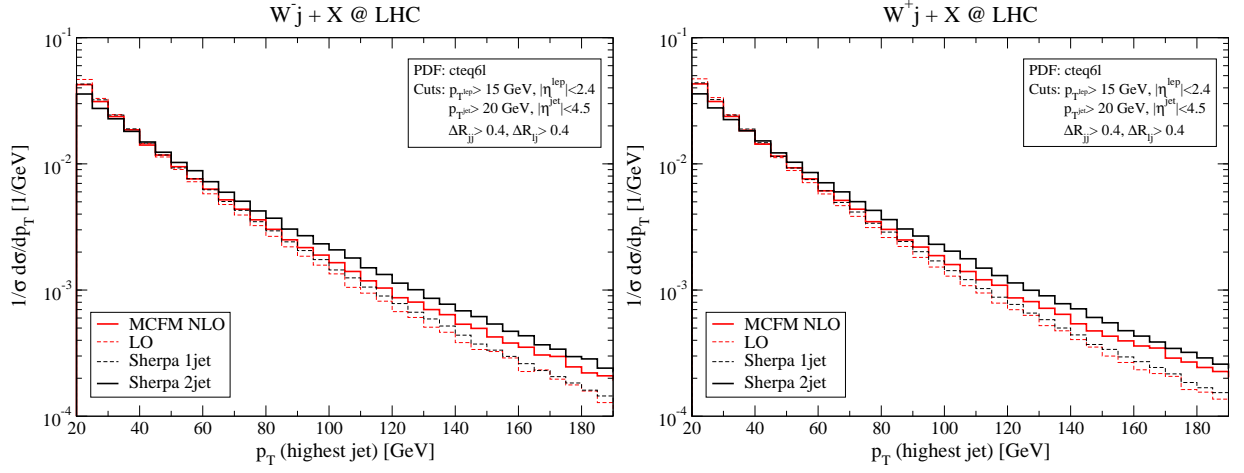


FIG. 9: The p_T distribution of the hardest jet for inclusive W^- (left panel) and W^+ (right panel) plus one jet events at the LHC.

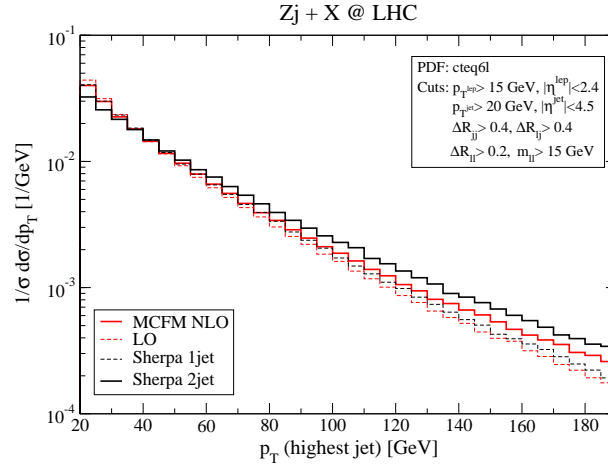


FIG. 10: The p_T distribution of the hardest jet for inclusive Z/γ^* plus one jet events at the LHC.

from SHERPA that were obtained with $n_{\max} = 1$ and with $n_{\max} = 2$, respectively. In all plots the high- p_{\perp} tail is significantly enhanced when going from LO to NLO. The SHERPA samples with $n_{\max} = 2$ show the same behavior but tend to pronounce the high- p_{\perp} region even more. This is in striking contrast to the $n_{\max} = 1$ samples. They are incapable of recovering the shape of the distribution at NLO, and tend to look like the LO result. This is not surprising. The NLO calculation takes into account tree-level matrix elements with two final state partons as the real contribution to the NLO result. Due to the large phase space available at the LHC this real contribution tends to produce an extra jet that alters the kinematics of the first jet. Obviously this significant change in the kinematics can not be appropriately recovered by the parton shower. The $n_{\max} = 2$ SHERPA samples also include the parton shower, resulting in increased parton emission thus enhancing the high- p_{\perp} tail even more. It would for sure be instructive to check this behaviour with a resummed NLO computation for these processes.

In Figs. 11 and 12 the p_{\perp} spectra of the two hardest jets in inclusive $W^+ + 2\text{jet}$, $W^- + 2\text{jet}$, and $Z/\gamma^* + 2\text{jet}$ production are displayed. This time next-to-leading order results from MCFM are compared with the corresponding SHERPA samples with $n_{\max} = 2$. It has been shown in [19] that the shapes of the distributions when going from LO to NLO are quite stable. The slopes of the next-to-leading order and the SHERPA result are in good agreement, the latter having the tendency to produce the first jet slightly harder. In Fig. 13 the p_{\perp} spectra of the two hardest jets in inclusive $W^- + 2\text{jet}$ production are displayed once more. This time, however, the renormalisation and factorisation scale in the NLO calculations has been chosen as $\mu_R = \mu_F = 2m_W$. For this choice of the scales the agreement of MCFM and SHERPA is even better. This highlights the effect of scale variations, a good way to estimate residual uncertainties

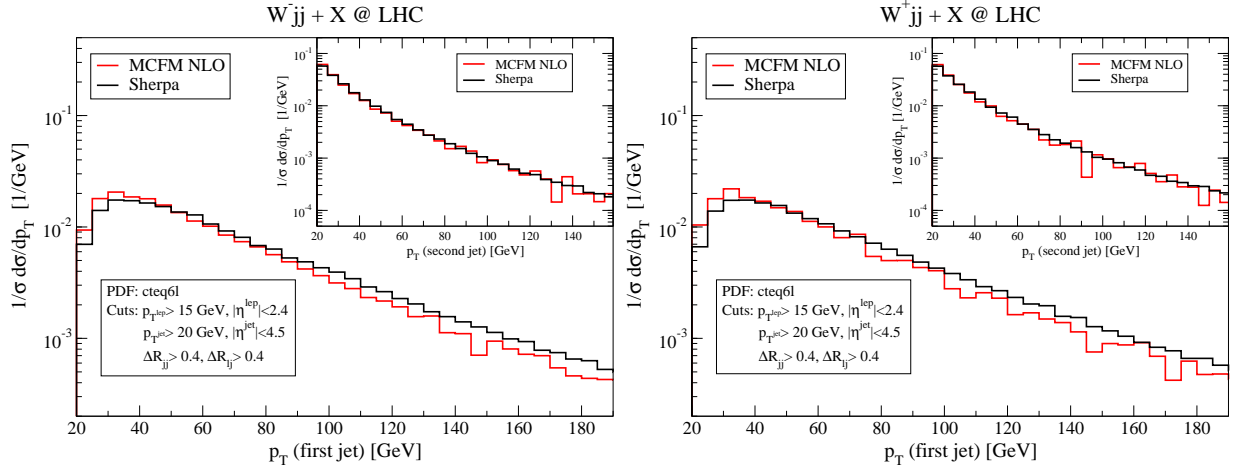


FIG. 11: The p_T distribution of the two hardest jets in inclusive W^- (left panel) and W^+ (right panel) plus two jet production at the LHC.

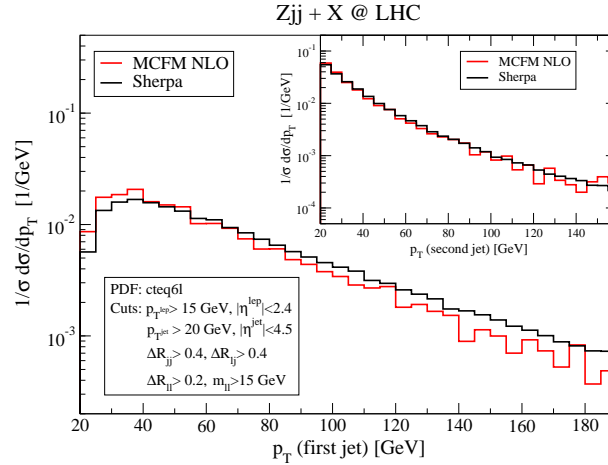


FIG. 12: The p_T distribution of the two hardest jets in inclusive Z/γ^* plus two jet production at the LHC.

due to higher order corrections and shows that the results of SHERPA are well within theoretical uncertainties ¹.

IV. SHERPA VS. MC@NLO AND PYTHIA

In this section, hadron-level results of SHERPA will be compared with those of two other event generators, namely MC@NLO [42, 43, 44] and PYTHIA [38, 39]. The former program incorporates a consistent matching of a full-fledged next-to-leading order calculation with the parton shower provided by HERWIG [40, 41]. It thus employs an angular-ordered shower, taking full account of coherence effects. In contrast, PYTHIA uses tree-level matrix elements, in this case for $q\bar{q} \rightarrow e^+e^-$ and it employs a virtuality-ordered parton shower to model further emissions. In this framework, coherence effects are approximated through an explicit veto on rising opening angles in the splitting. Hence, the parton shower implementations of PYTHIA and SHERPA are quite similar. However, in order to account in PYTHIA for jets with a p_\perp larger than the “natural” starting scale of the parton shower equal to the invariant mass of the lepton

¹ It should be noted that the effect of this scale variation on the total cross section merely is of the order of 1%, although the shape of the distribution in the high- p_\perp tail changes considerably.

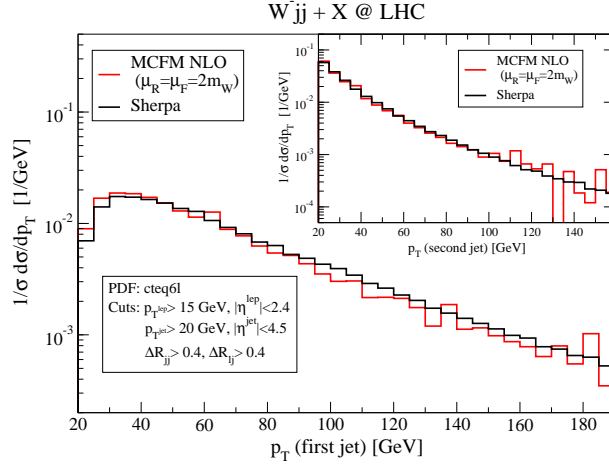


FIG. 13: The p_T distribution of the first and second hardest jet in inclusive W^- plus two jet production at the LHC. For the NLO calculation the renormalisation and factorisation scale have been chosen to $\mu_R = \mu_F = 2m_W$.

pair, the starting scale has been increased to the centre-of-mass energy of the proton-proton system, i.e. to 14 TeV. This choice is supplemented with a matrix element correction procedure implemented through reweighting meant to reproduce the exact matrix element for the emission of an additional jet. The precise setups for both codes can be found in appendix B.

First of all, the results of the three programs for some rather inclusive quantities are compared. The transverse momentum and pseudo-rapidity distributions of the produced bosons are presented in Fig. 14 and Fig. 15. The SHERPA predictions depicted have been obtained with $n_{\max} = 1$ and $Q_{\text{cut}} = 20$ GeV, in order to match the approaches of the other codes. In order to compare the different samples, they all have been subject to a cut on the boson invariant mass of the form

$$m_V - 30 \cdot \Gamma_V \leq m_V^* \leq m_V + 30 \cdot \Gamma_V, \quad (1)$$

where no additional phase space cuts have been applied. All distributions have been normalised to their respective cross section.

The results for both processes look very similar. The boson transverse momentum distributions of MC@NLO and SHERPA agree fairly well. In the case of Z/γ^* production they match nearly perfectly for values of $p_\perp > 100$ GeV. In the intermediate range of $10 \text{ GeV} < p_\perp < 100 \text{ GeV}$ SHERPA apparently is below MC@NLO. This discrepancy may have its origin in the different shower approaches used within the two programs. This statement is also hinted at by the fact that the PYTHIA result follows the SHERPA distribution for $p_\perp < 35$ GeV. For larger values of p_\perp , however, the PYTHIA distribution is far below MC@NLO and SHERPA predicting much less bosons with large transverse momentum. For the case of W^+ production the MC@NLO and SHERPA prediction cross at $p_\perp \approx 60$ GeV. SHERPA produces slightly less events with smaller boson p_\perp and tends to pronounce the high p_\perp region a bit. Again PYTHIA produces fewer bosons with intermediate and large boson transverse momenta. Looking at the pseudo-rapidity distributions, it can be recognized, that MC@NLO and SHERPA both tend to produce the bosons much more central than PYTHIA. Especially the region of $|\eta| < 4$ is filled significantly with respect to PYTHIA, which, in contrast, features a much broader shape. This effect is of course directly correlated to the larger amount of hard QCD radiation the other two programs produce, since this enhanced QCD radiation allows for larger boson recoils. Moreover, from Fig. 3 it can be anticipated how the SHERPA results change under the inclusion of matrix elements with extra QCD legs: the boson transverse momentum distribution develops a more pronounced large p_\perp tail and the very central region of η is filled even more, thus reducing the amount of events with large values of $|\eta|$. So while the p_\perp spectra would be slightly harder than those of MC@NLO the η distributions would fit even better than they do for the case of including $V+0$ and $V+1$ parton matrix elements only.

For the comparison of jet observables, only the case of Z/γ^* production is studied. The qualitative statements implied by it, however, will hold true as well in the case of W production. To judge the abilities of the three programs to produce extra hard QCD radiation associated to the electro-weak gauge bosons, the transverse momentum distributions of the three hardest jets are depicted in Fig. 16 and Fig. 17. For this comparison in addition to the cut on the boson transverse mass according to Eq. (1) the jet criteria and phase space cuts of appendix A have been applied. For SHERPA the jet resolution parameter has been set to $Q_{\text{cut}} = 20$ GeV. The standard sample for this comparison uses again only

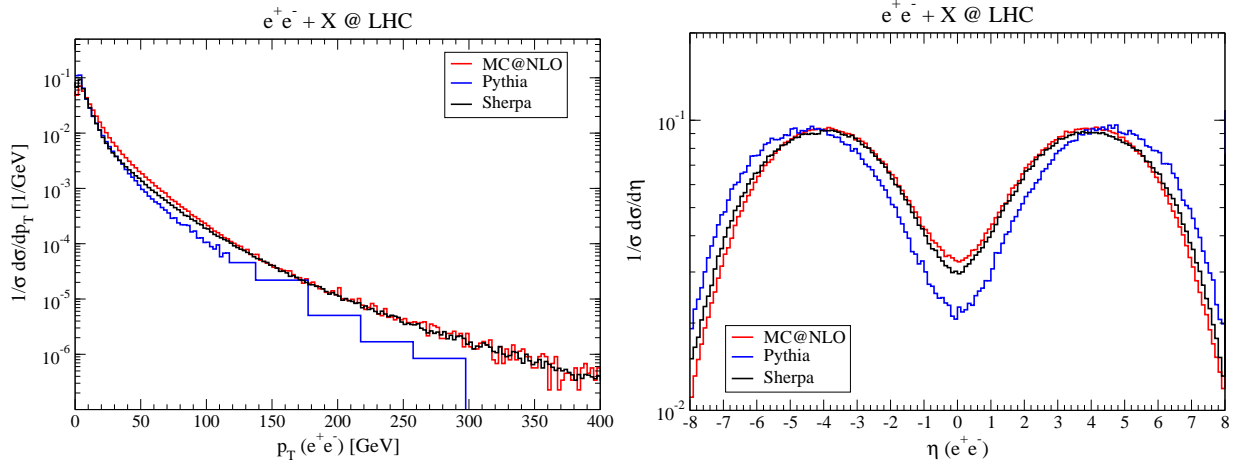


FIG. 14: The p_{\perp} (left) and η (right) distribution of the lepton pair in inclusive production of a Z/γ^* boson decaying into e^+e^- at the LHC. The results of the generators MC@NLO (red), PYTHIA (blue), and SHERPA (black) are compared.

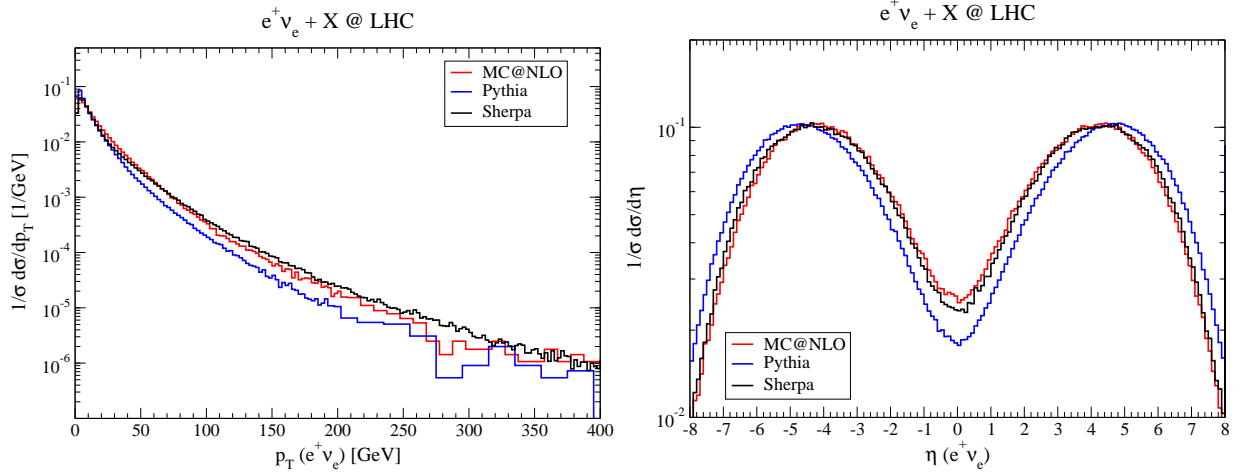


FIG. 15: The W^+ p_{\perp} (left) and η (right) distribution in inclusive production at the LHC. The results of the generators MC@NLO (red), PYTHIA (blue), and SHERPA (black) are compared.

matrix elements with up to one additional parton. To test the predictions of SHERPA samples with $n_{\max} = 2(3)$ have been considered as well, the corresponding results are shown as dashed (dotted) lines in the plots. Since it is actually the production rate that is important here, this time the curves have not been normalized. Instead the corresponding differential cross sections are presented.

For the hardest jet the predictions of MC@NLO and SHERPA agree rather well. The total rate of SHERPA is 12% smaller than that predicted by MC@NLO, the distribution, however, has a slightly harder tail. This difference in rate can be traced back to the different inclusive production cross sections. However, for $n_{\max} = 2$, the two total cross sections of $Z + 1\text{jet}$ nearly coincide (cf. the dashed black curve in Fig. 16). In terms of shape, SHERPA apparently favours jets with larger transverse momentum. As has been seen in the closely related boson p_{\perp} distribution in Fig. 14, PYTHIA predicts a much smaller rate (60% w.r.t. the rate predicted by MC@NLO) for the production of extra hard QCD radiation with a softer distribution.

For the second jet the situation changes significantly. Here, even in the case of including only matrix elements with up to one extra parton the two-jet rate predicted by SHERPA is 17% larger than that of MC@NLO. Including matrix elements with two extra partons the difference becomes nearly 90%. As for the case of the first jet, PYTHIA predicts the radiation of a second jet with a much smaller rate. Similar statements hold true when looking at the third jet but this time the differences are even larger. Note, that a reliable prediction of the three jet rate requires the inclusion of matrix elements with at least three extra partons. While the sample with matrix elements up to one extra parton

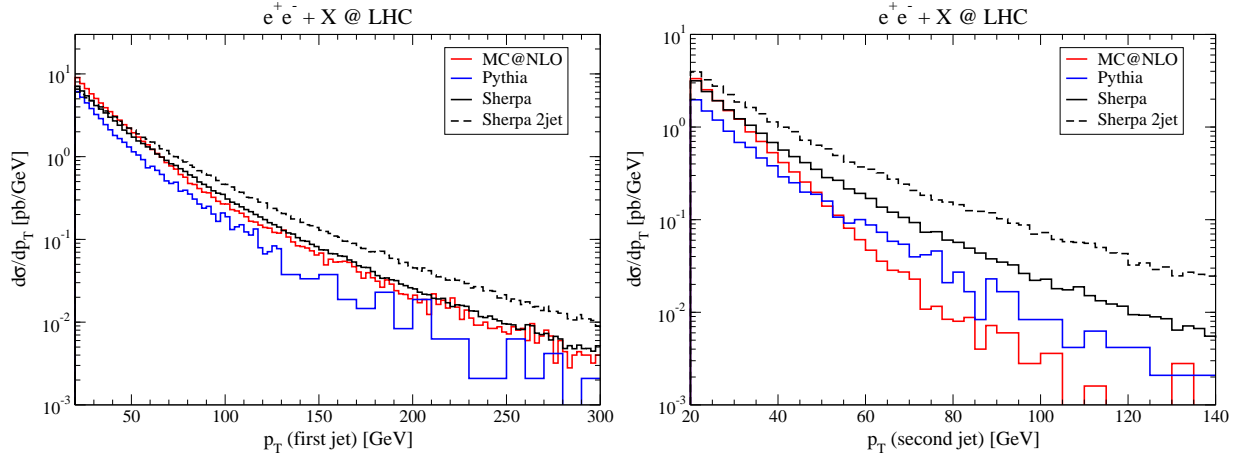


FIG. 16: The p_{\perp} distribution of the first (left) and second (right) hardest jet in inclusive Z/γ^* production at the LHC as obtained by MC@NLO (red), PYTHIA (blue) and SHERPA (black). The dashed curves correspond to the predictions of SHERPA when matrix elements for up to two additional partons are used.

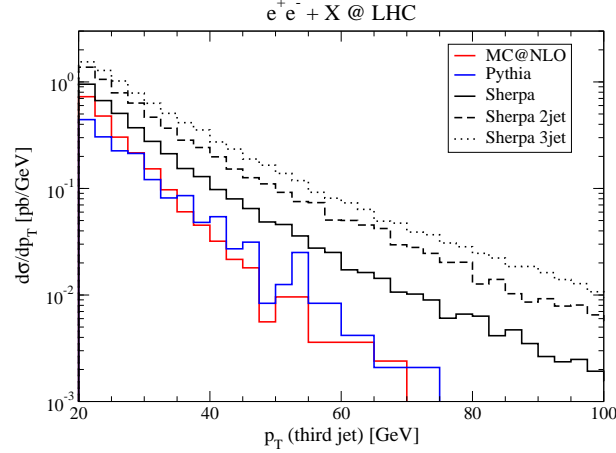


FIG. 17: The p_{\perp} distribution of the third hardest jet in inclusive Z/γ^* production at the LHC as obtained by MC@NLO (red), PYTHIA (blue) and SHERPA (black). The dashed (dotted) curve corresponds to the prediction of SHERPA when matrix elements for up to two (three) additional partons are used.

predicts a three jet rate of 9.6 pb, the samples with two (three) extra partons predict 16.3 (21.1) pb. However, this is not surprising keeping in mind that the LHC provides enough phase space to produce massive bosons in association with a multitude of high energetic jets that are best described by the corresponding matrix elements and that can not be appropriately described by parton shower emissions.

To summarize: the predictions of MC@NLO and SHERPA agree fairly well for the shape of the boson transverse momentum and pseudo-rapidity distribution. Here, MC@NLO is of course superior in predicting the rate of inclusive Z/γ^* and W production since it considers the corresponding production process at NLO in the coupling constant. This situation changes when studying the jets that potentially accompany the boson. As soon as more than one extra jet is considered SHERPA predicts significantly larger jet production rates and jet transverse momentum distributions that feature an enhanced population of the high- p_{\perp} region. Concerning PYTHIA it has to be stated that the shape of the boson transverse momentum and the boson pseudo-rapidity distribution differ significantly from the two other programs. This is directly related to the smaller amount of hard radiation produced by PYTHIA, clearly observed in the jet p_{\perp} spectra.

V. SUMMARY

In this publication, the previous validation of the merging procedure of matrix elements and the parton shower, as implemented in **SHERPA**, has been continued. Again, processes of the type $pp \rightarrow V + X$, where $V = W^\pm, Z/\gamma^*$ have been chosen; this time, however, the analysis focused on the case of the CERN LHC rather than on the Fermilab Tevatron. Again, the merging procedure turned out to yield sufficiently stable results over a wide range of internal parameters, rendering it a predictive way of incorporating the full information available in tree-level matrix elements into multi-purpose event generators, as anticipated. In addition, when comparing the results obtained through **SHERPA** with those of a full next-to-leading order calculation, it again turned out that the results of **SHERPA** reproduce the essential features in the NLO shapes. However, it should be stressed that in **SHERPA** the total rates are still at leading order accuracy only. Nevertheless, the fact that **SHERPA** seems to reproduce the NLO shapes of the observables, the NLO rates can be recovered by simply multiplying with a constant K -factor. When comparing the results of **SHERPA** with those of other event generators, some differences appear. Especially for observables sensitive to the correct treatment of multi-particle final states these differences have become significant, ranging up to orders of magnitude. In this study, **SHERPA** again proved its versatility in simulating high-multiplicity final states at collider experiments. Due to the merging procedure implemented in it, it provides a unique tool for the simulation of final states, where the proper treatment of the event topology is of great importance.

Acknowledgments

The authors would like to thank T. Gleisberg, S. Höche, and J. Winter for pleasant collaboration on **SHERPA** and M. L. Mangano and J. Campbell for helpful discussions. Financial support by BMBF, DESY-PT, GSI, and DFG is gratefully acknowledged.

APPENDIX A: INPUT PARAMETERS AND PHASE-SPACE CUTS

For all analyses, the PDF set cteq6l [20] has been used, and α_S has been chosen according to the corresponding value of this PDF, namely $\alpha_S = 0.118$. For the running of the strong coupling constant, the corresponding two-loop equation has been employed. Jets or initial partons are restricted to the light flavor sector, namely g, u, d, s , and c . All flavors are taken to be massless.

1. SM input parameters

The SM parameters are given in the G_μ scheme:

$$\begin{aligned} m_W &= 80.419 \text{ GeV}, & \Gamma_W &= 2.06 \text{ GeV}, \\ m_Z &= 91.188 \text{ GeV}, & \Gamma_Z &= 2.49 \text{ GeV}, \\ G_\mu &= 1.16639 \times 10^{-5} \text{ GeV}^{-2}, \\ \sin^2 \theta_W &= 1 - m_W^2/m_Z^2, \\ \alpha_s &= 0.118. \end{aligned} \tag{A1}$$

The electromagnetic coupling is derived from the Fermi constant G_μ according to

$$\alpha_{\text{em}} = \frac{\sqrt{2} G_\mu M_W^2 \sin^2 \theta_W}{\pi}. \tag{A2}$$

The constant widths of the electroweak gauge bosons are introduced through the fixed-width scheme. CKM mixing of the quark generations is neglected.

2. Cuts and jet criteria

For all jet analysis the Run II k_\perp clustering algorithm defined in [57] has been used. The additional parameter of this jet algorithm is a pseudo-cone size R , whose value has been chosen to $R = 0.4$. In addition jets have to fulfil the

following cuts on transverse momentum and pseudo-rapidity,

$$p_T^{\text{jet}} > 20 \text{ GeV}, \quad |\eta^{\text{jet}}| < 4.5. \quad (\text{A3})$$

For charged leptons the cuts applied are:

$$p_T^{\text{lepton}} > 15 \text{ GeV}, \quad |\eta^{\text{lepton}}| < 2.4, \quad m_{ll} > 15 \text{ GeV}. \quad (\text{A4})$$

No cut on missing transverse momentum has been applied.

The final selection criteria correspond to the separation of the leptons amongst each other and with respect to the jets,

$$\Delta R_{lj} > 0.4, \quad \Delta R_{ll} > 0.2. \quad (\text{A5})$$

APPENDIX B: SETUPS FOR MC@NLO AND PYTHIA

- **The MC@NLO setup:** The program version used is MC@NLO 2.31. The process number corresponding to $pp \rightarrow Z/\gamma^* \rightarrow e^+e^- + X$ production is `IPROC=-11351`, for $pp \rightarrow W^+ \rightarrow e^+\nu_e + X$ this equals `IPROC=-11461`. In both cases consequently the underlying event has been switched off. The lepton pair in Z/γ^* production has been generated in a mass window of

$$m_Z - 30\Gamma_Z \leq m_{ee} \leq m_Z + 30\Gamma_Z \quad (\text{B1})$$

in the case of W^+ production the lepton-neutrino pair fulfils

$$m_W - 30\Gamma_W \leq m_{e\nu_e} \leq m_W + 30\Gamma_W \quad (\text{B2})$$

The PDF set used is `cteq6l`. All other physics parameters that specify a run for MC@NLO have been left unchanged with respect to their default values.

- **The PYTHIA setup:** The PYTHIA version used is 6.214. The process $pp \rightarrow Z/\gamma^* + X$ is selected via the parameter `MSUB(1)=1`. The decay mode $Z/\gamma^* \rightarrow e^+e^-$ is picked by the settings `MDME(182,1)=1` and `MDME(170,1)=1`, all other decay channels have been disabled. The process $pp \rightarrow W^+ + X$ is turned on via `MSUB(2)=1`. The decay mode $W^+ \rightarrow e^+\nu_e$ is chosen by `MDME(206,1)=1`. It has proven to be convenient to increase the standard value of the shower starting scale in PYTHIA to $\sqrt{s} = 14 \text{ TeV}$ in order to produce a reasonable amount of high energetic QCD radiation. The parameter responsible for controlling the shower start scales is `MSTP(68)`. For the above choice it has set to `MSTP(68)=2`. All other parameters specific for PYTHIA have been left unaltered, except that PYTHIA's underlying event has been switched off.

-
- [1] G. Altarelli, R. K. Ellis and G. Martinelli, Nucl. Phys. B **157** (1979) 461.
 - [2] J. Kubar-Andre and F. E. Paige, Phys. Rev. D **19** (1979) 221.
 - [3] K. Harada, T. Kaneko and N. Sakai, Nucl. Phys. B **155** (1979) 169 [Erratum, ibid. B **165** (1980) 545].
 - [4] J. Abad and B. Humpert, Phys. Lett. B **80** (1979) 286.
 - [5] B. Humpert and W. L. Van Neerven, Phys. Lett. B **85** (1979) 293.
 - [6] R. Hamberg, W. L. van Neerven and T. Matsuura, Nucl. Phys. B **359** (1991) 343 [Erratum, ibid. B **644** (2002) 403].
 - [7] R. V. Harlander and W. B. Kilgore, Phys. Rev. Lett. **88** (2002) 201801 [arXiv:hep-ph/0201206].
 - [8] C. Anastasiou, L. J. Dixon, K. Melnikov and F. Petriello, Phys. Rev. D **69** (2004) 094008 [arXiv:hep-ph/0312266].
 - [9] C. Balazs and C. P. Yuan, Phys. Rev. D **56** (1997) 5558 [arXiv:hep-ph/9704258].
 - [10] F. A. Berends, H. Kuijff, B. Tausk and W. T. Giele, Nucl. Phys. B **357** (1991) 32.
 - [11] A. Pukhov *et al.*, arXiv:hep-ph/9908288.
 - [12] T. Ishikawa, T. Kaneko, K. Kato, S. Kawabata, Y. Shimizu and H. Tanaka [MINAMI-TATEYA group Collaboration], KEK-92-19
 - [13] K. Sato *et al.*, Proc. VII International Workshop on Advanced Computing and Analysis Techniques in Physics Research (ACAT 2000), P. C. Bhat and M. Kasemann, AIP Conference Proceedings **583** (2001) 214.
 - [14] T. Stelzer and W. F. Long, Comput. Phys. Commun. **81** (1994) 357 [arXiv:hep-ph/9401258].
 - [15] F. Maltoni and T. Stelzer, JHEP **0302** (2003) 027 [arXiv:hep-ph/0208156].
 - [16] M. L. Mangano, M. Moretti, F. Piccinini, R. Pittau and A. D. Polosa, JHEP **0307** (2003) 001 [arXiv:hep-ph/0206293].

- [17] F. Krauss, R. Kuhn and G. Soff, JHEP **0202**, 044 (2002) [arXiv:hep-ph/0109036].
- [18] J. Campbell and R. K. Ellis, Phys. Rev. D **65** (2002) 113007 [arXiv:hep-ph/0202176].
- [19] J. Campbell, R. K. Ellis and D. L. Rainwater, Phys. Rev. D **68** (2003) 094021 [arXiv:hep-ph/0308195].
- [20] J. Pumplin, D. R. Stump, J. Huston, H. L. Lai, P. Nadolsky and W. K. Tung, JHEP **0207** (2002) 012 [arXiv:hep-ph/0201195].
- [21] V. A. Khoze, A. D. Martin, R. Orava and M. G. Ryskin, Eur. Phys. J. C **19** (2001) 313 [arXiv:hep-ph/0010163].
- [22] M. Dittmar, F. Pauss and D. Zurcher, Phys. Rev. D **56** (1997) 7284 [arXiv:hep-ex/9705004].
- [23] A. D. Martin, R. G. Roberts, W. J. Stirling and R. S. Thorne, Eur. Phys. J. C **14** (2000) 133 [arXiv:hep-ph/9907231].
- [24] W. T. Giele and S. A. Keller, arXiv:hep-ph/0104053.
- [25] ATLAS Collaboration, “Detector and Physics Performance Technical Design Report”, CERN/LHCC/99-15, vol. 2.
- [26] S. Haywood *et al.*, arXiv:hep-ph/0003275.
- [27] S. Abachi *et al.* [D0 Collaboration], Phys. Rev. Lett. **75** (1995) 1456 [arXiv:hep-ex/9505013].
- [28] T. Affolder *et al.* [CDF Collaboration], Phys. Rev. D **64** (2001) 052001 [arXiv:hep-ex/0007044].
- [29] V. M. Abazov *et al.* [D0 Collaboration], Phys. Rev. D **66** (2002) 012001 [arXiv:hep-ex/0204014].
- [30] W. Ashmanskas *et al.*, the Tevatron Electroweak Working Group, CDF and D0 Collaborations, arXiv:hep-ex/0311039.
- [31] C. Albajar *et al.* [UA1 Collaboration], Phys. Lett. B **253** (1991) 503.
- [32] J. Alitti *et al.* [UA2 Collaboration], Phys. Lett. B **276** (1992) 365.
- [33] F. Abe *et al.* [CDF Collaboration], Phys. Rev. D **52** (1995) 2624.
- [34] B. Abbott *et al.* [D0 Collaboration], Phys. Rev. D **61** (2000) 072001 [arXiv:hep-ex/9906025].
- [35] T. Affolder *et al.* [CDF Collaboration], Phys. Rev. Lett. **85** (2000) 3347 [arXiv:hep-ex/0004017].
- [36] V. M. Abazov *et al.* [D0 Collaboration], Phys. Rev. D **66** (2002) 032008 [arXiv:hep-ex/0204009].
- [37] F. Krauss, A. Schälicke, S. Schumann and G. Soff, Phys. Rev. D **70** (2004) 114009 [arXiv:hep-ph/0409106].
- [38] T. Sjöstrand, Comput. Phys. Commun. **82** (1994) 74;
- [39] T. Sjöstrand, L. Lönnblad and S. Mrenna, arXiv:hep-ph/0108264.
- [40] G. Corcella *et al.*, JHEP **0101** (2001) 010 [arXiv:hep-ph/0011363].
- [41] G. Corcella *et al.*, arXiv:hep-ph/0210213.
- [42] S. Frixione and B. R. Webber, JHEP **0206** (2002) 029 [arXiv:hep-ph/0204244].
- [43] S. Frixione, P. Nason and B. R. Webber, JHEP **0308** (2003) 007 [arXiv:hep-ph/0305252].
- [44] S. Frixione and B. R. Webber, arXiv:hep-ph/0402116.
- [45] T. Gleisberg, S. Höche, F. Krauss, A. Schälicke, S. Schumann and J. C. Winter, JHEP **0402** (2004) 056 [arXiv:hep-ph/0311263].
- [46] M. H. Seymour, Comput. Phys. Commun. **90** (1995) 95 [hep-ph/9410414].
- [47] G. Miu and T. Sjöstrand, Phys. Lett. B **449** (1999) 313 [hep-ph/9812455].
- [48] G. Corcella and M. H. Seymour, Nucl. Phys. B **565** (2000) 227 [hep-ph/9908388].
- [49] S. Catani, Y. L. Dokshitzer, M. Olsson, G. Turnock and B. R. Webber, Phys. Lett. B **269** (1991) 432.
- [50] S. Catani, Y. L. Dokshitzer and B. R. Webber, Phys. Lett. B **285** (1992) 291.
- [51] S. Catani, Y. L. Dokshitzer, M. H. Seymour and B. R. Webber, Nucl. Phys. B **406** (1993) 187.
- [52] S. Catani, F. Krauss, R. Kuhn and B. R. Webber, JHEP **0111** (2001) 063 [arXiv:hep-ph/0109231].
- [53] F. Krauss, JHEP **0208** (2002) 015 [arXiv:hep-ph/0205283].
- [54] L. Lönnblad, JHEP **0205** (2002) 046 [arXiv:hep-ph/0112284].
- [55] S. Mrenna and P. Richardson, JHEP **0405** (2004) 040 [arXiv:hep-ph/0312274].
- [56] M. L. Mangano, M. Moretti and R. Pittau, Nucl. Phys. B **632** (2002) 343 [arXiv:hep-ph/0108069].
- [57] G. C. Blazey *et al.*, arXiv:hep-ex/0005012.